ACS Catalysis

Research Article

pubs.acs.org/acscatalysis

Catalytic Cycle of Penicillin Acylase from *Escherichia coli*: QM/MM Modeling of Chemical Transformations in the Enzyme Active Site upon Penicillin G Hydrolysis

Bella L. Grigorenko,[†,‡] Maria G. Khrenova,[†] Dmitry K. Nilov,[§] Alexander V. Nemukhin,*[,†,‡] and Vytas K. Švedas*[,§,∥]

[†]Chemistry Department, Lomonosov Moscow State University, 1-3 Leninskiye Gory, Moscow 119991, Russia

[‡]Emanuel Institute of Biochemical Physics, Russian Academy of Sciences, 4 Kosygin Street, Moscow 119991, Russia

[§]Belozersky Institute of Physicochemical Biology, Lomonosov Moscow State University, Leninskie Gory, Moscow 119991, Russia

[∥]Faculty of Bioengineering and Bioinformatics, Lomonosov Moscow State University, 1-73 Leninskie Gory, Moscow 119991, Russia

Supporting Information

ABSTRACT: Penicillin acylase from *Escherichia coli* is a unique enzyme that belongs to the recently discovered superfamily of N-terminal nucleophile hydrolases. It catalyzes selective hydrolysis of the side chain amide bond of penicillins and cephalosporins while leaving the labile amide bond in the *β*-lactam ring intact. Despite wide applications of penicillin acylase in the industry of *β*-lactam antibiotics and production of chiral amino compounds, its catalytic mechanism at atomic resolution has not yet been characterized. The complete cycle of chemical transformations of the most specific substrate of the enzyme, penicillin G, leading to formation of 6-aminopenicillanic and phenylacetic acids was modeled following quantum mechanics−molecular mechanics (QM/MM) calculations of the minimum energy reaction profile. The active site residues and the substrate were included in the QM part, and the rest of the system was treated applying molecular mechanics and classical force field parameters. The 3D structures in the enzyme active site corresponding to the noncovalent enzyme−substrate complex, the covalent acylenzyme intermediate, the noncovalent enzyme−product complex, the tetrahedral intermediates, and the respective transition states have been identified. QM/MM studies have shown that the *α*-amino group of the N-terminal catalytic *β*Ser1 plays a key role in the catalytic machinery and directly assists its hydroxyl group in a proton relay at major stages of penicillin acylase catalytic mechanism, formation and hydrolysis of the covalent acylenzyme intermediate, which are characterized by close energy barriers. The *β*Ser1 residue together with the oxyanion hole residues *β*Ala69 and *β*Asn241 as well as *β*Arg263 and *β*Gln23 constitute a buried active site interaction network responsible for stabilization of tetrahedral intermediates, transition states, orientation of substrate and catalytic residues. *β*Arg263 and *β*Gln23 maintain the integrity of the catalytic machinery: *β*Arg263 participates in orientation of the substrate as well as the *α*-amino group of *β*Ser1 and coordinates the oxyanion hole residue *β*Asn241 across the whole catalytic cycle, whereas the backbone of *β*Gln23 is responsible for orientation of both the *β*Ser1 and the substrate. These results deliver insight into the earlier unknown ability of N-terminal amino acid to activate its own nucleophilic group directly as well as into organization of the stabilizing interaction network in penicillin acylase's active site and will be used to design more effective enzyme variants for synthesis of new penicillins and cephalosporins.

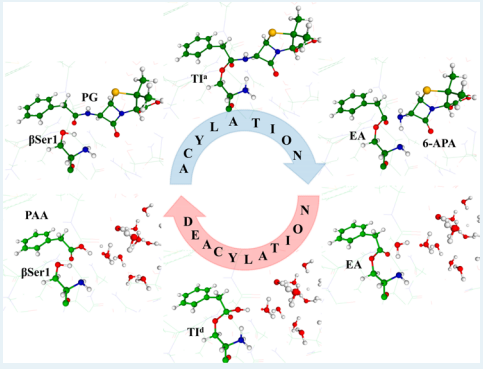

KEYWORDS: *penicillin acylase, N-terminal nucleophile hydrolases, molecular modeling, reaction mechanism, QM/MM*

INTRODUCTION

Penicillin acylases (PA) are enzymes highly attractive for biotechnological applications. They play a crucial role in the industry of the most widely used *β*-lactam antibiotics due to the exclusive ability to catalyze selective hydrolysis or synthesis of the side chain amide bond while leaving the labile amide bond in the *β*-lactam ring intact.[1−4] Penicillin acylases can also catalyze effective and enantioselective acylation/deacylation of amino compounds in aqueous medium and can be used to produce individual enantiomers of nonconventional amino acids, primary amines, amino alcohols, and aminonitriles or protection/deprotection of amino groups in peptide synthesis.[5−14]

These enzymes are members of the N-terminal nucleophile (Ntn) hydrolase superfamily,[15,16] which is characterized by involvement of the N-terminal amino acid (serine, threonine, or

Received: March 4, 2014
Revised: May 5, 2014
Published: June 23, 2014

   dx.doi.org/10.1021/cs5002898 | ACS Catal. 2014, 4, 2521−2529

cysteine) in the catalytic machinery. In contrast to well-studied serine proteases[17] and hydrolases[18] that operate due to formation of the catalytic triad Ser−His−Asp(Glu) in the enzyme active site, the Ntn hydrolases do not contain a catalytic triad or dyad. In the crystal structure of PA from *Escherichia coli*, determined at 1.9 Å resolution (PDB code: 1PNK),[19] there was no adjacent histidine to the N-terminal catalytic βSer1, and the nearest base to the βSer1 hydroxyl group was its own N-terminal amino group. It led to the suggestion that this α-amino group can enhance the nucleophile reactivity of βSer1 through the bridging water molecule as a virtual base.

Quantum chemical modeling of the molecular system composed of fragments of the PA active site corresponded with the suggested role of the N-terminal amino acid in the catalytic mechanism and confirmed that the amino group of the N-terminal serine in Ntn hydrolases is capable of activating its own hydroxyl group. However, in contrast to the proposed involvement of a bridging water molecule in a proton shuttling, it was demonstrated that direct assistance of the α-amino group of the N-terminal serine in activation of its own hydroxyl group can be more effective. Calculations at the ab initio quantum chemistry level have also shown a substantial impact of a specific solvation of the tetrahedral intermediate in an oxyanion hole that can decrease the activation barrier at formation of the acylenzyme by approximately 10 kcal/mol.[20] The important role of the oxyanion hole residues βAla69, βAsn241, and βGln23 (using 1PNK numbering) was demonstrated by structural studies[21] as well as QSAR studies and molecular mechanical modeling of PA-catalyzed reactions.[22,23] One more indirect evidence questioning the involvement of a bridging water molecule is related to structural studies when no water molecule adjacent to the βSer1 Oγ was observed in a PA complex with a very slowly hydrolyzable substrate analogue, penicillin G sulfoxide.[24]

Although the crucial role of the N-terminal βSer1 in PA catalysis is widely recognized, the detailed mechanism at atomic resolution is still speculative and not supported by strict evidence. Methods of theoretical chemistry can be used to answer this question. When modeling enzymatic reactions (i.e., the processes of cleavage and formation of chemical bonds of substrates inside protein matrices) the combined quantum mechanical−molecular mechanical (QM/MM) approach is a method of choice.[25−27] In this technique, a part of the entire model system containing reagents with the nearest molecular groups is ascribed to the QM part and a larger part of the system is considered as the MM part. Energies and energy gradients with respect to nuclear coordinates in the QM subsystem, where chemical transformations are supposed to take place, are computed by using methods of quantum chemistry. Energies and forces in the MM subsystem are evaluated using classical force field parameters. Location of the stationary points on the potential energy surface corresponding to the geometric configurations of reagents, products, transition states, and possible intermediates provides valuable information on the reaction pathways.

In this work, the QM/MM modeling of the chemical transformations in the course of PA-catalyzed penicillin G (PG) hydrolysis to 6-aminopenicillanic acid (6-APA) and phenylacetic acid (PAA) (Scheme 1) was performed in order to clarify the role of the active site residues across the whole catalytic cycle.

Scheme 1. PA-Catalyzed Selective Hydrolysis of the Side Chain Amide Bond of PG to 6-Aminopenicillanic Acid (6-APA) and Phenylacetic Acid (PAA) while Leaving the Labile Amide Bond in the β-Lactam Ring Intact

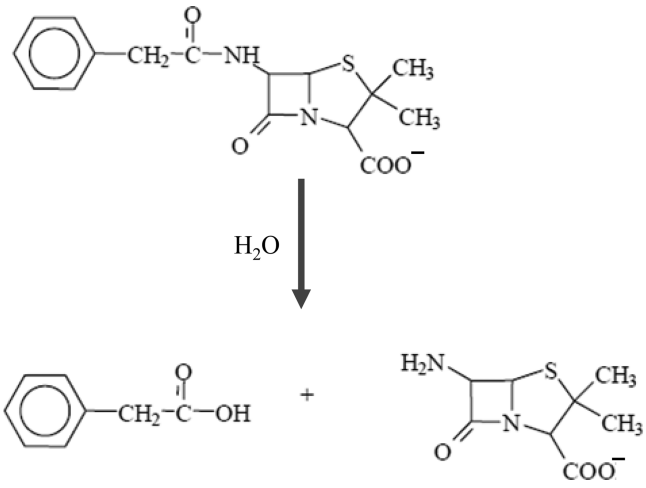

Our primary goal was to locate stationary points on the potential energy surface corresponding to the noncovalent enzyme−substrate (ES) complex, the covalent acylenzyme (EA) intermediate, the noncovalent enzyme−product (EP) complex, tetrahedral intermediates (TI), and the corresponding transition states (TS), as well as to identify the relevant 3D structures in the enzyme active site.

MODELS AND METHODS

The minimum energy profile of the PA's catalytic cycle was computed by using the flexible effective fragment variant[28,29] of the QM/MM approach. In this method, the MM subsystem is represented by a collection of effective fragments (EFs) whose contributions to the quantum Hamiltonian of the QM part are extended far beyond simple electrostatics through the partial charges on MM atoms.[30,31] Namely, EFs from the MM subsystem contribute their electrostatic potentials expanded up to octupoles to the quantum Hamiltonian. These one-electron electrostatic contributions as well as contributions from interactions of polarizable EFs with the QM part are obtained in the preliminary calculations using the quantum chemical electron densities. The exchange-repulsion potentials which are combined with the electrostatic and polarizability terms are also created in the preliminary quantum based calculations. Therefore, all empirical parameters are entirely within the MM subsystem. This version of the QM/MM method is implemented, in particular, in the GAMESS(US) program suite.[32,33]

Calculation of energy and forces in the QM part was carried out with the density functional theory version PBE0/6-31G*. The PBE0 functional[34,35] was selected because of its good overall performance.[36] Calculation results for selected stationary points on the potential energy surface were confirmed by using different quantum chemistry approaches. Corresponding technical details and calculation results are presented in Sections S1 and S2 of the Supporting Information. Energies and forces in the MM subsystem were estimated by using the TINKER program[37] with the AMBER force field parameters.[38]

The X-ray structure of PA complex with a very slowly hydrolyzable substrate analogue, penicillin G sulfoxide (PDB code: 1GM9),[26] was chosen as an initial source of coordinates

dx.doi.org/10.1021/cs5002898 | ACS Catal. 2014, 4, 2521−2529

of heavy atoms. Recently performed modeling of PA binding with penicillin G (PG) using molecular dynamics simulations have shown that 1GM9 structure most adequately corresponds to the productive enzyme−substrate complex.[39] In this work, we manually replaced penicillin G sulfoxide by the "true" substrate PG in the 1GM9 structure and added hydrogen atoms to the amino acid residues by assuming ordinary protonation states of the polar groups: negatively charged Asp and Glu, and positively charged Lys and Arg. Protonation states of the histinide residues were assigned manually by considering their hydrogen bonding patterns; in particular, βHis192, closest to the active site, was protonated at N_δ and deprotonated at N_ε. In prior QM/MM optimization of equilibrium geometry parameters of the model molecular system, we carried out a series of MM minimization runs to clean the structure. We verified that arrangement of the substrate and the residues in the active site is consistent with conclusions of previous molecular dynamics simulations.[39]

Atoms of the substrate, βSer1, and the side chain of βArg263 were assigned to the QM subsystem. The latter was treated at the quantum level because of the expected strong electrostatic effect of the charged group located in the immediate vicinity of an area where cleavage and formation of chemical bonds take place. As explained in Sections S1−S3 of Supporting Information, we also considered extended choices of quantum subsystems for a part of the reaction profile showing that the major conclusions of the work were not dependent on the calculation details.

Structures of the noncovalent enzyme−substrate (ES) complex, the covalent acylenzyme (EA) intermediate, and the noncovalent enzyme−product (EP) complex, as well as those of tetrahedral intermediates (TI) were obtained in series of unconstrained QM/MM minimizations. To estimate positions of the saddle points, the respective transition states (TS), separating those minimum energy areas on the potential energy surface, we selected appropriate reaction coordinates described below, and for each value of the corresponding geometry parameter, we optimized all other coordinates in the QM/MM system. We traced the sign of the energy gradient with respect to the assumed reaction coordinate, and the change of this sign indicated that the system was in the vicinity of TS. When the saddle points were located , we have verified that the descent forward and backward correctly led to the respective minimum energy structures. As described in Section S1 of Supporting Information, properties of the saddle point structure TS1[a] are confirmed by vibrational analysis showing single imaginary frequency.

For brevity, we further omit symbol β as an identification of the chain β in the protein structure 1PNK, because all residues discussed below refer to this chain only.

RESULTS

Active Site Structures along the Reaction Pathway: Enzyme−Substrate Complex. QM/MM optimized structure of the enzyme−substrate complex and characteristic distances between heavy atoms are depicted in Figure 1. The aromatic ring is tightly bound in the hydrophobic pocket, and polar groups are involved in the active site interaction network. An important role in PG orientation belongs to amino acid residues that constitute a hydrogen bonding around the substrate and Ser1: the side chains of Ala69 and Asn241 form the oxyanion hole, the positively charged side chain of Arg263 coordinates the α-amino group of Ser1 and the carbonyl group of the β-lactam ring, the backbone NH of Gln23 forms a hydrogen bond with Oγ of Ser1, and the backbone oxygen coordinates NH group of the scissile amide bond of PG along the reaction pathway until formation of acylenzyme intermediate. We notice two key distances that indicate disposition of N-terminal α-amino group: 2.50 Å between Oγ of Ser1 and the carbonyl carbon of the substrate, and 2.51 Å between Oγ and the nitrogen of the α-amino group of Ser1.

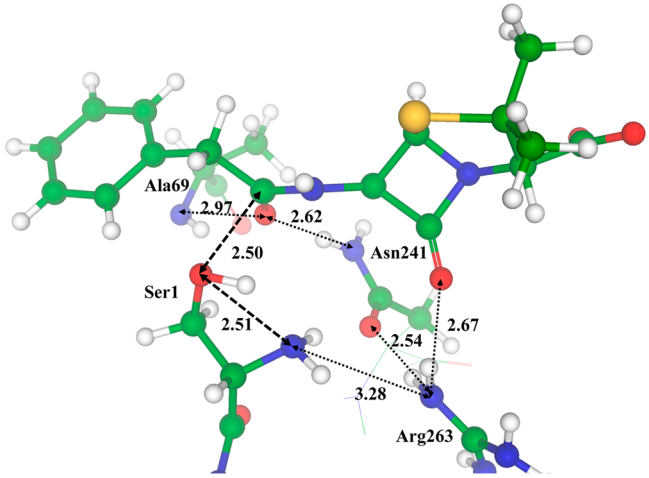

Figure 1. Substrate binding and orientation in the enzyme active site. Here and in all other figures carbon atoms are colored in green, oxygen in red, nitrogen in blue, sulfur in yellow; the distances are given in angstroms.

Active Site Structures along the Reaction Pathway: Tetrahedral Intermediate at the Acylation Stage. The reaction coordinate on the route from ES to the first tetrahedral reaction intermediate formed at the acylation stage (TI[a]) was selected as a distance between the Oγ atom of Ser1 and the side chain carbonyl carbon atom of PG. The first transition state (TS1[a]) structure in QM/MM calculations was located by gradually reducing this distance from the initial value 2.50 Å (see Figure 1) and optimizing all other geometry parameters. The N−H distance in Ser1 was further selected as a reaction coordinate to estimate location of the second transition state (TS2[a]), the saddle point separating TI[a] and the covalent acylenzyme intermediate (EA[a]). QM/MM studies have identified that acylation stage of the PA-catalyzed PG hydrolysis consists of four steps:

(i) proton shuttling from Oγ to the α-amino group of Ser1 concerted with a nucleophilic attack of the activated Ser1 on the PG side chain carbonyl group composing the first transition state TS1[a] (Figure 2, left inset);
(ii) formation of the tetrahedral intermediate stabilized in the oxyanion hole by Ala69 and Asn241 residues (Figure 2);
(iii) composition of the second transition state TS2[a] followed by a proton transfer from the protonated α-amino group of Ser1 in the tetrahedral intermediate to the amino group of the first reaction product (Figure 2, right inset);
(iv) formation of the covalent acylenzyme intermediate and the first reaction product 6-aminopenicillanic acid.

The unconstrained minimization toward formation of the covalent EA intermediate allowed us to identify changes in the characteristic distances between the key atoms along the reaction pathway. Consecutive reduction of the Oγ(Ser)−C(PG) distance from 2.50 Å in the noncovalent ES complex to

dx.doi.org/10.1021/cs5002898 | ACS Catal. 2014, 4, 2521−2529

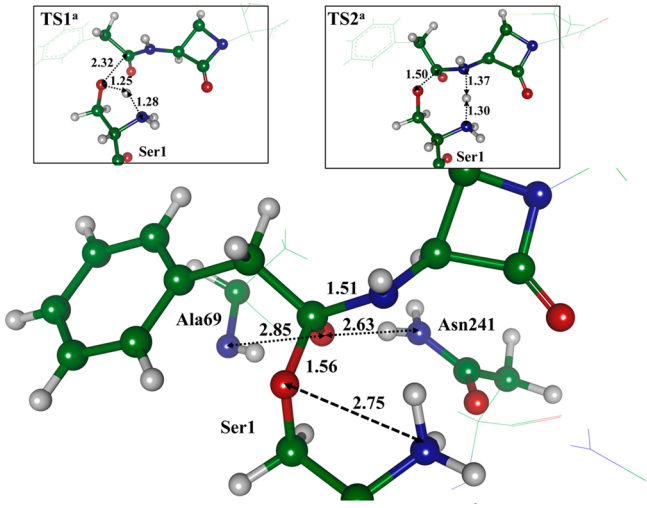

Figure 2. Structural fragment of the tetrahedral intermediate TI[a] formed at the acylation stage. The insets illustrate distances between the key atoms in the transition state geometry configurations separating TI[a] from ES (TS1[a]) and EA[a] (TS2[a]).

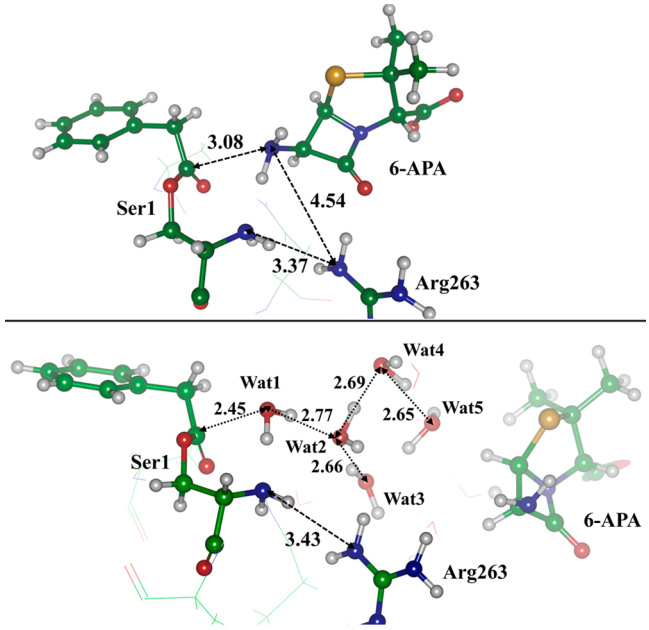

Figure 3. Model structures of the acylenzyme (EA) complex with the first reaction product 6-APA formed at the acylation stage (upper panel) and EA complex with water molecules at deacylation stage (bottom panel).

2.32 Å in the first transition state TS1[a], then to 1.56 Å in the tetrahedral intermediate TI[a] and to 1.50 Å in the second transition state TS2[a] is taking place. The elongation of the C(PG)−N(PG) distance from 1.38 Å in ES to 1.51 Å upon formation of TI[a] also should be noted. Observed intermolecular rearrangements are accompanied by respective shuffling in the hydrogen bonding network that favors chemical transformations in the enzyme active site: in particular, the proton stays nearly equidistant between Oγ and the α-amino group of Ser1 in the first transition state TS1[a] to facilitate nucleophilic attack, the distance between the nitrogen atom of the oxyanion hole residue Ala69 and the carbonyl oxygen of PG is reduced from 2.97 Å in ES to 2.85 Å to stabilize TI[a], and the α-amino group of Ser1 in the second transition state TS2[a] is ready to donate proton to the amino group of 6-aminopenicillanic acid (6-APA)—the first product formed after cleavage of the amide bond. The backbone of Gln23 participates in stabilization of the tetrahedral intermediate.

It is important to note that in the catalytic mechanism that is suggested on the basis of the crystal structure of PA, the bridging water molecule was supposed to mediate the proton transfer between the Oγ atom of Ser1 and its own α-amino group to enhance nucleophile reactivity.[19] QM/MM studies demonstrate that water molecule is not involved in the catalytic machinery, and the α-amino group of N-terminal serine directly assists the hydroxyl group to activate it.

Active Site Structures along the Reaction Pathway: Covalent Acylenzyme Intermediate. The products formed at the acylation stage and characteristic distances between the key atoms are depicted in Figure 3 (the upper panel).

The side chain C−N bond in PG is cleaved: the corresponding distance between the carbonyl carbon and the nitrogen atom of 6-APA amino group gradually increased from 1.38 Å in ES to 1.51 Å in TI[a] (see Figure 2) and finally to 3.08 Å leading to the formation of the covalent reaction intermediate EA[a] (the covalent Oγ(Ser)−C bond formed is 1.33 Å) and 6-APA. The energy of this model system is 14.5 kcal/mol below the initial level of ES.

In order to simulate chemical transformations of the deacylation stage, the model system was reconstructed as follows: the 6-APA molecule was removed from the PA's active site, and the cavity was filled with water molecules. It is consistent with kinetic data reported earlier that 6-APA is poorly bound in the PA's active site.[40,41] The corresponding model system EA[d], which is depicted in Figure 3 (bottom panel), demonstrates involvement of water molecules in the partially shown hydrogen bonding network.

Active Site Structures along the Reaction Pathway: Tetrahedral Intermediate at the Deacylation Stage. The reaction coordinate on the route from EA[d] to the second tetrahedral intermediate (TI[d]) was selected as a distance between the oxygen atom of the attacking water molecule Wat1 and the carbonyl carbon atom of the acylenzyme. The third transition state (TS1[d]) structure in QM/MM calculations was located by gradually reducing this distance from the initial value of 2.45 Å in the covalent acylenzyme intermediate (see Figure 3) to 1.88 Å (Figure 4, left inset) and optimizing all other geometry parameters. The unconstrained minimization toward EA hydrolysis (deacylation) allowed us to reach points corresponding to the TI[d] structure (Figure 4, mainframe). The fourth transition state TS2[d] (Figure 4, right inset), separating the minimum energy geometry configuration TI[d] from the second reaction product, was located by manually transporting the proton from the α-amino group to the Oγ atom of N-terminal Ser1. Similarly to the formation of the covalent acylenzyme intermediate, the deacylation stage also consists of four steps:

(i) nucleophilic attack of Wat1 on the carbonyl group of EA resulting in the third transition state TS1[d] followed by a proton transfer from the attacking Wat1 to the α-amino group of Ser1 (Figure 4, left inset);
(ii) formation of the second tetrahedral intermediate TI[d] stabilized in the oxyanion hole by Ala69 as well as Asn241 residues (Figure 4, primary image) and orientation of the Asn241 side chain carbonyl group by the α-amino group of Ser1 and Arg263 residue;

dx.doi.org/10.1021/cs5002898 | ACS Catal. 2014, 4, 2521−2529

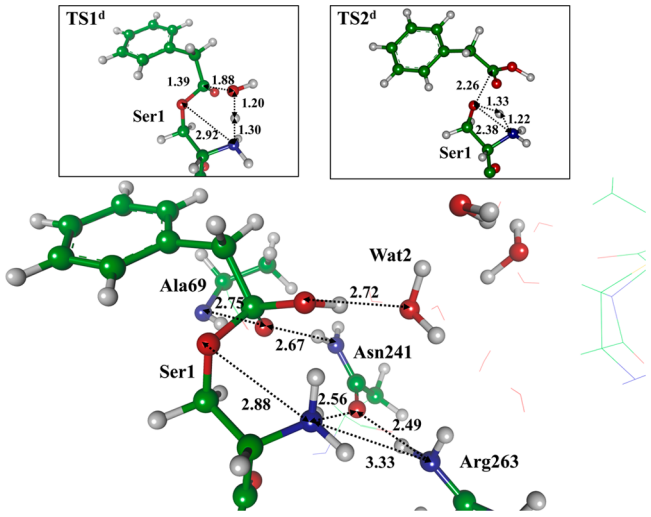

Figure 4. Fragment of the tetrahedral intermediate at the deacylation stage, TI^d. The upper insets illustrate characteristic distances between the key atoms in the geometry configurations of the third and fourth transition states $TS1^d$ and $TS2^d$.

(iii) attainment of the fourth transition state $TS2^d$, in which the proton is nearly equidistant between the Oγ atom and nitrogen of the α-amino group of Ser1 (Figure 4, right inset);

(iv) formation of the noncovalent complex of enzyme with the second reaction product phenylacetic acid followed by a final proton transfer to the Oγ atom of Ser1 and regeneration of the active enzyme (Figure 5).

Active Site Structures along the Reaction Pathway: Enzyme–Product Complex. QM/MM modeling clearly demonstrates the key role and direct participation of the α-amino group of N-terminal Ser1 in the proton shuttling back to the Oγ atom of Ser1 at the deacylation stage of the PA-catalyzed PG hydrolysis. When the proton translocation from the attacking water molecule through formation of $TS1^d$, TI^d, and $TS2^d$ is completed, the second product of the reaction, phenylacetic acid, is formed (Figure 5). The energy of this model system is only 2 kcal/mol below the level of EA^d. Although the covalent acylenzyme intermediate is hydrolyzed, thus regenerating the hydroxyl group in the side chain of Ser1 and allowing the enzyme to be ready to enter the next catalytic cycle, phenylacetic acid tends not to leave the active site and forms a quite stable noncovalent EP complex due to the high affinity to PA. The next catalytic cycle of PG hydrolysis can nevertheless be initiated by the second substrate molecule, because PG has a higher affinity by about 1 order of magnitude compared to the phenylacetic acid[40] and therefore can push the product out of the PA's active site.

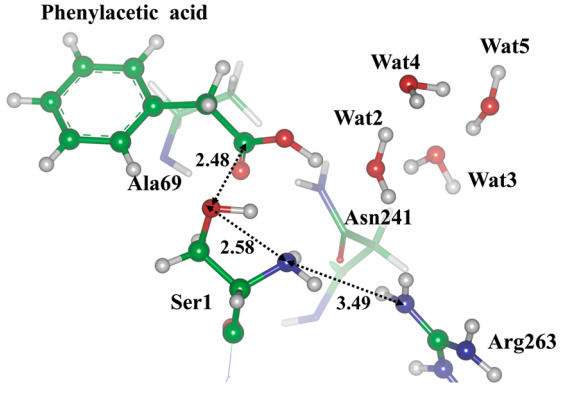

Figure 5. Characteristic distances between heavy atoms in the enzyme complex with the second reaction product phenylacetic acid formed at hydrolysis of the covalent EA intermediate (the deacylation stage).

Energy Diagram. QM/MM modeling has shown that the PA-catalyzed PG hydrolysis consists of several steps with very moderate energy barriers as a result of the stabilization of transition states and tetrahedral intermediates in the enzyme active site. The crucial role in the stabilization belongs to oxyanion hole residues Ala69 and Asn241, as well as to coordinating residues Gln23 and Arg263, whereas the α-amino group of N-terminal Ser1 directly participates in the activation of its own hydroxyl group and plays a crucial role in proton shuttling across the whole catalytic cycle.

The calculated minimum energy profile of PA-catalyzed PG hydrolysis (Figure 6) demonstrates the gradual decrease in energy along the reaction pathway: ES → TI^a → EA → TI^d → EP. The highest potential energy barriers between the elementary steps of the reaction refer to formation of the transitions state structures from the tetrahedral intermediates: $TS2^d$ (7.3 kcal/mol from the level of TI^d) and $TS2^a$ (5.5 kcal/mol from the level of TI^a). Formation of the first transition state $TS1^a$ from the enzyme–substrate complex ES constitutes 5.1 kcal/mol.

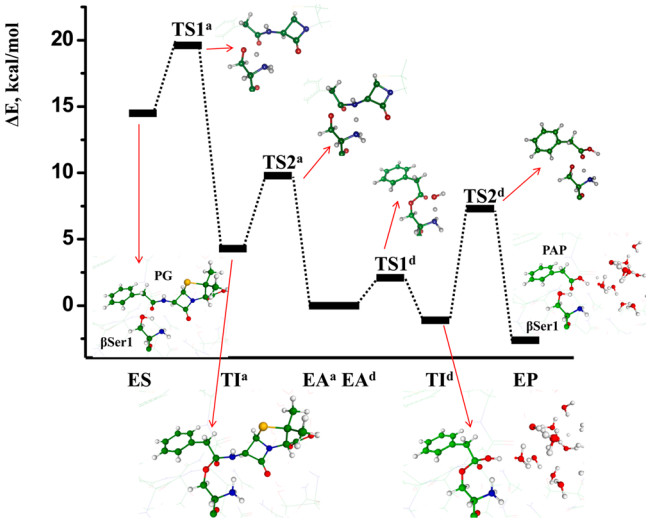

Figure 6. Computed energy diagram of the PA-catalyzed hydrolysis of PG. The energies of the EA^a and EA^d model systems that contain different amount of water molecules have been equalized and set to zero. Structures at the stationary points are better visualized in Figures 1–5; Scheme 2 below illustrates corresponding transformations in chemical terms.

We analyzed decomposition of the overall QM/MM energy values along the reaction profile as well as sensitivity of the calculation results to the details of computational approaches taking the very first reaction step ES → $TS1^a$ → TI^a as a representative example. As described in a Section S3 of the Supporting Information, the energies of $TS1^a$ and TI^a (relative to the level of ES) computed by quantum chemistry tools are estimated to be unrealistically high (15–20 kcal/mol) without contributions from the surrounding molecular groups of the MM parts. Addition of the electrostatic contributions from the

dx.doi.org/10.1021/cs5002898 | ACS Catal. 2014, 4, 2521–2529

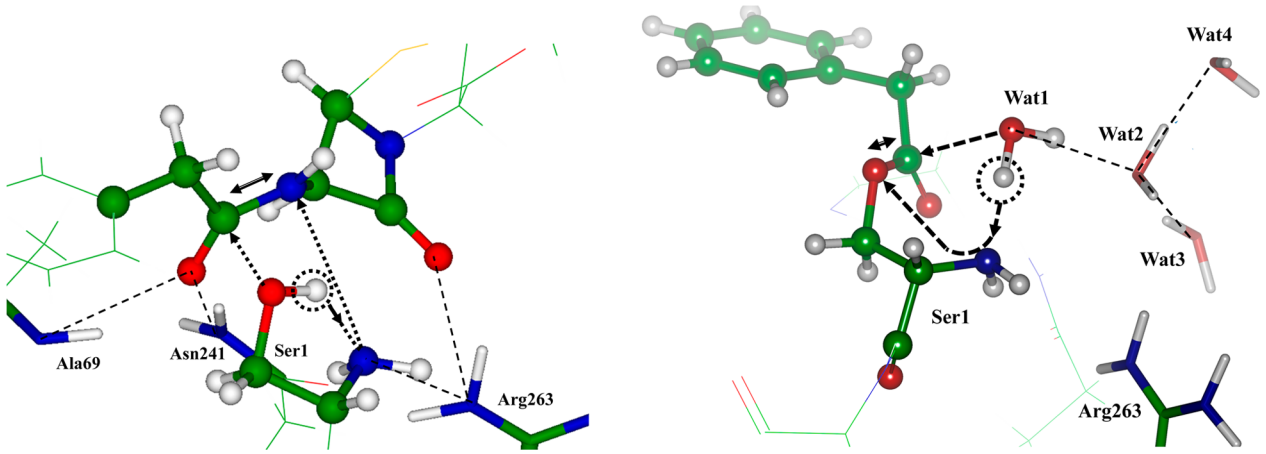

Figure 7. Scheme of the acylation (left) and deacylation (right) stages of the PA-catalyzed hydrolysis of PG. Dotted lines illustrate directions of attacks of the reacting species. The protons circled by dotted lines are directly transmitted by the amino group of Ser1.

MM part to the quantum Hamiltonian matrices (i.e., application of the electronically embedded QM/MM methodology)[27] dramatically improves the energies. It demonstrates that selective hydrolysis of the side chain amide bond of penicillin G to 6-aminopenicillanic acid and phenylacetic acid while leaving the labile amide bond in the β-lactam ring intact is possible only when substrate is properly bound and oriented in the enzyme active site due to integrity of the buried active site interaction network responsible for stabilization of tetrahedral intermediates, transition states, orientation of substrate, and catalytic residues. Model systems that do not take into account all interactions of the substrate and the active site residues cannot adequately model this unique catalytic ability of penicillin acylase. In fact, chemical hydrolysis of penicillin G to these products in aqueous solution is not possible because the labile amide bond in the β-lactam ring is hydrolyzed much faster.

Although the focus of this work was mainly on the role of the active site residues in PA catalysis, we emphasize that the computed minimum energy reaction profile is consistent with the energy changes within 10 kcal/mol at all elementary steps as expected for enzymatic processes. The QM/MM modeling has shown that activation energies at the acylation and deacylation stages should be comparable, amounting to 6−8 kcal/mol at the potential energy scale. Entropic contributions to energy differences, especially to the activation free energies, must be taken into account to bridge the gap between modeling and experimental data. These contributions cannot be easily computed at the same accuracy level as applied here for the minimum potential energy profile. According to the relevant estimates for chemical reactions in the enzyme active site and in solution,[42,43] the values of about 2−3 kcal/mol are expected to correct potential barriers on the reaction profiles due to entropic component. In PA catalysis, entropic contributions are expected to be more pronounced at the deacylation rather than at the acylation stage, because the reagents and intermediates on the route from EA to EP are more solvent-exposed. By all means, a direct comparison of the experimental and computational data when relying on the transition state theory that relates the free energy activation energy and the rate constant is complicated for processes that include several consecutive elementary steps. The results of the QM/MM simulations are consistent with the experimental data of 10.2 kcal/mol, which is obtained in Arrhenius approximation to the temperature dependence of the PA-catalyzed PG hydrolysis.

DISCUSSION

Molecular modeling of elementary stages of enzymatic reactions by using modern computational tools including QM/MM approaches is continuously expanding. However, a complete cycle of chemical transformations in the enzyme active site covering all steps of substrate conversion to products is very rarely reported. In this work, we are able to construct the entire reaction profile at the uniform theoretical level and to characterize the full cycle of catalytic events inside the penicillin acylase active center at atomic resolution. The QM/MM modeling of PA-catalyzed PG hydrolysis has shown an earlier unknown role of N-terminal Ser1 residue and its amino group in activation of catalytic residue in the enzyme active site. The α-amino group of N-terminal Ser1 is one of the key elements of penicillin acylase catalytic machinery at both acylation and deacylation stages (Figure 7). At the acylation stage, the α-amino group of N-terminal Ser1 directly participates in activation of its own hydroxyl group (Figure 7, left panel), and this proton shuttling from Oγ to the α-amino group of Ser1 (as shown by dashed lines) is concerted with a nucleophilic attack of activated Ser1 on the PG side chain carbonyl group and generation of the first transition state followed by formation of the first tetrahedral intermediate.

The proton carried by the α-amino group of Ser1 in the tetrahedral intermediate and in the second transition state is further transferred to the amino group of the 6-aminopenicillanic acid (first reaction product) produced at formation of the covalent acylenzyme intermediate. At the deacylation stage (Figure 7, right panel) the N-terminal α-amino group activates the nucleophilic water molecule by accepting its proton and directly transferring it to Oγ of Ser1. Thus, it was shown that the α-amino group can shuttle the proton along the catalytic pathway directly without participation of the bridging water molecule, as was suggested earlier on a basis of the X-ray structure determined at 1.9 Å resolution (PDB code: 1PNK).[19]

The role of the positively charged residue in the PA active site first evidenced from experimental studies of the enantioselective PA-catalyzed hydrolysis of *N*-phenylacetylated amino acids[44] was clarified and demonstrated to belong to Arg263. Arg263 is a necessary component of the stabilizing interaction network at the acylation stage (Figure 7, left panel)

dx.doi.org/10.1021/cs5002898 | *ACS Catal.* 2014, 4, 2521−2529

Scheme 2. Illustration of the Key Steps and the Role of the Crucial Amino Acid Residues in the Catalytic Mechanism Based on QM/MM Modeling of the PA-Catalyzed Hydrolysis of PG

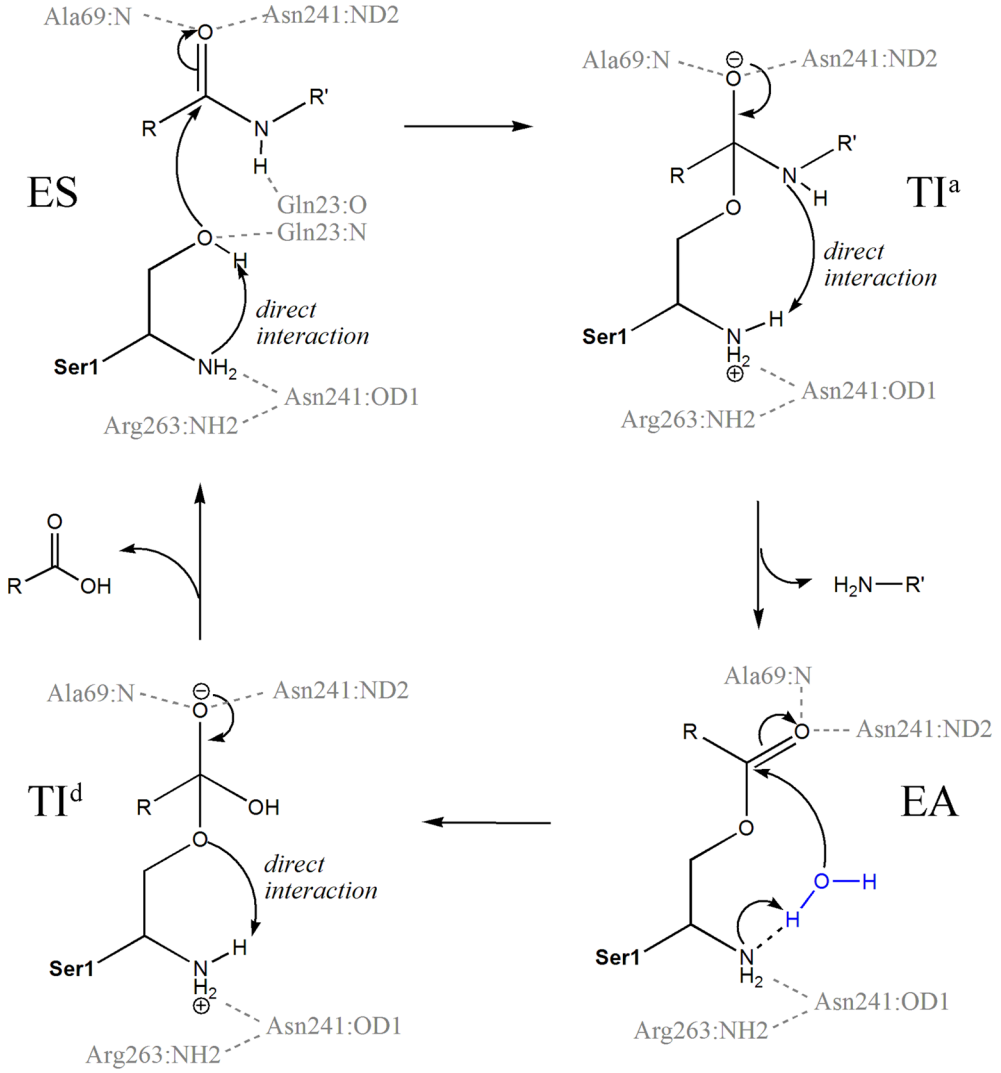

and participates in orientation of the substrate (PG) by interacting with the β-lactam carbonyl group (distances of Arg263:HH1···PNN:O_{ring} are 1.61 Å in ES, 1.67 Å in TI[a], 1.61 Å in EA[a]) as well as of the α-amino group of Ser1. The Arg263 residue also coordinates one of the oxyanion hole residues Asn241 across the whole catalytic cycle, especially at the deacylation stage and formation of the second reaction product: distances between the Asn241:OD and Arg263:HH2 are 1.92 Å in ES, 1.70 Å in TI[a], 1.78 Å in EA[a], 1.55 Å in EA[d], 1.58 Å in TI[d], 1.54 Å in EP.

An important role in substrate orientation also belongs to amino acid residues that together with the positively charged side chain of Arg263 constitute a hydrogen bonding network around the substrate and Ser1: Ala69 and the side chain of Asn241 form the oxyanion hole, and the backbone of Gln23 participates in the orientation of Ser1 and the substrate. Interaction between the α-amino group of Ser1, Arg263, and the side chain carbonyl group of Asn241 provides integrity of the catalytic machinery. Involvement of the crucial amino acid residues in the catalytic mechanism as determined by QM/MM modeling of the PA-catalyzed hydrolysis of PG is illustrated in Scheme 2.

It is interesting to compare the PA catalytic mechanism with that of β-lactamases also converting penicillins and responsible for microbial resistance to β-lactam antibiotics. Their catalytic mechanism was recently studied by molecular modeling tools including QM/MM.[45−49] Serine β-lactamase hydrolyzes the more labile amide bond of PG's β-lactam ring and activates its active site Ser70 residue for nucleophilic attack by side chain Glu166 acting as the general base through an intervening conserved water molecule.[47] This reaction can be effectively performed as well by metallo-dependent β-lactamases;[50] however, no Ntn hydrolases are known to have β-lactamase activity, and vice versa, no metallo-dependent enzymes are known to hydrolyze the more stable side chain amide bond in β-lactam antibiotics. The problem of regiospecific conversion of penicillins and cephalosporins in microbial systems is solved by employing enzymes from different superfamilies that exploit different catalytic mechanisms.

CONCLUSION

Molecular modeling of PA-catalyzed hydrolysis of penicillin G allowed us to locate structures of the noncovalent enzyme−substrate complex, the covalent acylenzyme intermediate, the noncovalent enzyme−product complex, the tetrahedral inter-

dx.doi.org/10.1021/cs5002898 | ACS Catal. 2014, 4, 2521−2529

mediates, and the respective transition states along the reaction pathway. The complete cycle of PA catalytic mechanism was characterized for the first time at the consistent theoretical level. The QM/MM studies have shown an earlier unknown role of N-terminal Ser1 residue and its amino group in activation of catalytic residue in the enzyme active site. The α-amino group of the N-terminal catalytic Ser1 directly assists its hydroxyl group in a proton relay at major stages of the PA catalytic mechanism—formation and hydrolysis of the covalent acylenzyme intermediate. The key role of the positively charged residue in the PA active site earlier evidenced from experimental studies was demonstrated to belong to Arg263, which is responsible for integrity of the stabilizing interaction network in the PA active site, participates in orientation of the substrate as well as the α-amino group of Ser1, and coordinates the oxyanion hole residue Asn241 across the whole catalytic cycle. The important element of the catalytic machinery is the backbone of Gln23 responsible for orientation of both the Ser1 and the substrate.

■ ASSOCIATED CONTENT

Ⓢ Supporting Information

Supporting Information contains details of various QM/MM protocols, decomposition of the computed QM/MM energies, estimates of entropic contributions to the energy profile. This material is available free of charge via the Internet at http://pubs.acs.org. The full set of coordinates for the structures reported in the paper in the pdb format is available from the authors upon request.

■ AUTHOR INFORMATION

Corresponding Authors

*E-mail: anemukhin@yahoo.com, anem@lcc.chem.msu.ru.
*E-mail: vytas@belozersky.msu.ru.

Notes

The authors declare no competing financial interest.

■ ACKNOWLEDGMENTS

This study was supported by the Russian Ministry for Science and Education (contract no. 02.527.11.0001) as a joint EU-Russian FP7 project "IRENE" (grant agreement no. 227279) and the Russian Foundation for Basic Research (project no. 13-03-00210). We acknowledge the use of supercomputer resources of the M.V. Lomonosov Moscow State University[51] and of the Joint Supercomputer Center of the Russian Academy of Sciences.

■ REFERENCES

(1) Elander, R. P. *Appl. Microbiol. Biotechnol.* **2003**, *61*, 385−392.
(2) Spence, D. W.; Ramsden, M. *Penicillin Acylases, Industrial Enzymes*; Polaina, J., MacCabe, A.P. , Eds.; Springer: Dordrecht, The Netherlands, 2007; pp 583−597.
(3) Arroyo, M.; De la Mata, I.; Acebal, C.; Castillón, M. P. *Appl. Microbiol. Biotechnol.* **2003**, *60*, 507−514.
(4) Bruggink, A.; Roos, E. C.; De Vroom, E. *Org. Process Res. Dev.* **1998**, *2*, 128−133.
(5) Soloshonok, V. A.; Fokina, N. A.; Rybakova, A. V.; Shishkina, I. P.; Galushko, S. V.; Sorochinsky, A. E.; Švedas, V. K. *Tetrahedron: Asymmetry* **1995**, *6*, 1601−1610.
(6) Carboni, C.; Kierkels, H. G. T.; Gardossi, L.; Tamiola, K.; Janssen, D. B.; Quaedflieg, P. J. L. M. *Tetrahedron: Asymmetry* **2006**, *17*, 245−251.
(7) Solodenko, V. A.; Belik, M. Y.; Galushko, S. V.; Kukhar, V. P.; Kozlova, E. V.; Mironenko, D. A.; Švedas, V. K. *Tetrahedron: Asymmetry* **1993**, *4*, 1965−1968.
(8) Chilov, G. G.; Moody, H. M.; Boesten, W. H.; Švedas, V. K. *Tetrahedron: Asymmetry* **2003**, *14*, 2613−2617.
(9) Guranda, D. T.; Van Langen, L. M.; Van Rantwijk, F.; Sheldon, R. A.; Švedas, V. K. *Tetrahedron: Asymmetry* **2001**, *12*, 1645−1650.
(10) Guranda, D. T.; Khimiuk, A. I.; Van Langen, L. M.; Van Rantwijk, F.; Sheldon, R. A.; Švedas, V. K. *Tetrahedron: Asymmetry* **2004**, *15*, 2901−2906.
(11) Guranda, D. T.; Ushakov, G. A.; Švedas, V. K. *Acta Naturae* **2010**, *2*, 94−97.
(12) Ismail, H.; Lau, R. M.; Van Langen, L. M.; Van Rantwijk, F.; Švedas, V. K.; Sheldon, R. A. *Green Chem.* **2008**, *10*, 415−418.
(13) Khimiuk, A. Y.; Korennykh, A. V.; Van Langen, L. M.; Van Rantwijk, F.; Sheldon, R. A.; Švedas, V. K. *Tetrahedron: Asymmetry* **2003**, *14*, 3123−3128.
(14) Švedas, V. K.; Beltser, A. I. *Ann. N.Y. Acad. Sci.* **1998**, *864*, 524−527.
(15) Brannigan, J. A.; Dodson, G.; Duggleby, H. J.; Moody, P. C.; Smith, J. L.; Tomchick, D. R.; Murzin, A. G. *Nature* **1995**, *378*, 416−419.
(16) Oinonen, C.; Rouvinen, J. *Protein Sci.* **2000**, *9*, 2329−2337.
(17) Hedstrom, L. *Chem. Rev.* **2002**, *102*, 4501−4524.
(18) Simon, G. M.; Cravatt, B. F. *J. Biol. Chem.* **2010**, *285*, 11051−11055.
(19) Duggleby, H. J.; Tolley, S. P.; Hill, C. P.; Dodson, E. J.; Dodson, G.; Moody, P. C. E. *Nature* **1995**, *373*, 264−268.
(20) Chilov, G. G.; Sidorova, A. V.; Švedas, V. K. *Biochemistry (Moscow)* **2007**, *72*, 495−500.
(21) Alkema, W. B.; Hensgens, C. M.; Kroezinga, E. H.; De Vries, E.; Floris, R.; Van der Laan, J. M.; Dijkstra, B. W.; Janssen, D. B. *Protein Eng.* **2000**, *13*, 857−863.
(22) Zhiryakova, D.; Ivanov, I.; Ilieva, S.; Guncheva, M.; Galunsky, B.; Stambolieva, N. *FEBS J.* **2009**, *276*, 2589−2598.
(23) Basso, A.; Braiuca, P.; Ebert, C.; Gardossi, L.; Linda, P.; Benedetti, F. *Biochim. Biophys. Acta* **2002**, *1601*, 85−92.
(24) McVey, C. E.; Walsh, M. A.; Dodson, G. G.; Wilson, K. S.; Brannigan, J. A. *J. Mol. Biol.* **2001**, *313*, 139−150.
(25) Warshel, A.; Levitt, M. *J. Mol. Biol.* **1976**, *103*, 227−249.
(26) Senn, H. M.; Thiel, W. *Angew. Chem., Int. Ed.* **2009**, *48*, 1198−229.
(27) Groenhof, G. *Methods Mol. Biol.* **2013**, *924*, 43−66.
(28) Grigorenko, B. L.; Nemukhin, A. V.; Topol, I. A.; Burt, S. K. *J. Phys. Chem. A* **2002**, *106*, 10663−10672.
(29) Nemukhin, A. V.; Grigorenko, B. L.; Topol, I. A.; Burt, S. K. *J. Comput. Chem.* **2003**, *24*, 1410−1420.
(30) Gordon, M. S.; Freitag, M. A.; Bandyopadhyay, P.; Jensen, J. H.; Kairys, V.; Stevens, W. J. *J. Phys. Chem. A* **2001**, *105*, 293−307.
(31) Gordon, M. S.; Slipchenko, L. V.; Li, H.; Jensen, J. H. *Ann. Rep. Comp. Chem.* **2007**, *3*, 177−193.
(32) Schmidt, M. W.; Baldridge, K. K.; Boatz, J. A.; Elbert, S. T.; Gordon, M. S.; Jensen, J. H.; Koseki, S.; Matsunaga, N.; Nguyen, K. A.; Su, S.; Windus, T. L.; Dupuis, M.; Montgomery, J. A. *J. Comput. Chem.* **1993**, *14*, 1347−1363.
(33) Gordon, M. S.; Schmidt, M. W. In *Theory and Applications of Computational Chemistry, the First Forty Years*; Dykstra, C. E., Frenking, G., Kim, K. S., Scuseria, G. E., Eds.; Elsevier: Amsterdam, 2005; pp 1167−1189.
(34) Perdew, J. P.; Burke, K.; Ernzerhof, M. *Phys. Rev. Lett.* **1996**, *77*, 3865−3868.
(35) Adamo, C.; Barone, V. *J. Chem. Phys.* **1999**, *110*, 6158−6170.
(36) Del Campo, J. M.; Gázquez, J. L.; Trickey, S. B.; Vela, A. *J. Chem. Phys.* **2012**, *136*, 104108.
(37) Ponder, J. W. *TINKER Molecular Modeling Package*, version 5.1; Washington University Medical School: St. Louis, MO, 2010.
(38) Case, D. A.; Cheatham, T.; Darden, T.; Gohlke, H.; Luo, R.; Merz, K. M.; Onufriev, A.; Simmerling, C.; Wang, B.; Woods, R. *J. Comput. Chem.* **2005**, *26*, 1668−1688.

(39) Novikov, F. N.; Stroganov, O. V.; Khaliullin, I. G.; Panin, N. V.; Shapovalova, I. V.; Chilov, G. G.; Švedas, V. K. *FEBS J.* **2013**, *280*, 115−126.
(40) Berezin, I. V.; Klyosov, A. A.; Nys, P. S.; Savitskaya, E. M.; Švedas, V. K. *Antibiotiki* **1974**, *19*, 880−887.
(41) Kutzbach, C.; Rauenbush, E. *Hoppe-Seyler's Z. Physiol. Chem.* **1974**, *355*, 45−53.
(42) Villà, J.; Štrajbl, M.; Glennon, T. M.; Sham, Y. Y.; Chu, Z. T.; Warshel, A. *Proc. Natl. Acad. Sci. U.S.A.* **2000**, *97*, 11899−11904.
(43) Štrajbl, M.; Sham, Y. Y.; Villà, J.; Chu, Z. T.; Warshel, A. *J. Phys. Chem. B* **2000**, *104*, 4578−4584.
(44) Švedas, V. K.; Savchenko, M. V.; Beltser, A. I.; Guranda, D. F. *Ann. N.Y. Acad. Sci.* **1996**, *799*, 659−669.
(45) Massova, I.; Kollman, P. A. *J. Comput. Chem.* **2002**, *23*, 1559−1576.
(46) Gherman, B. F.; Goldberg, S. D.; Cornish, V. W.; Friesner, R. A. *J. Am. Chem. Soc.* **2004**, *23*, 7652−7664.
(47) Hermann, J. C.; Hensen, C.; Ridder, L.; Mulholland, A. J.; Höltje, H. D. *J. Am. Chem. Soc.* **2005**, *127*, 4454−4465.
(48) Sharma, S.; Bandyopadhyay, P. *J. Mol. Model.* **2012**, *18*, 481−492.
(49) Kumarasiri, M.; Zhang, W.; Shi, Q.; Fisher, J. F.; Mobashery, S. *Proteins* **2014**, *82*, 1348−1358.
(50) Díaz, N.; Suárez, D.; Merz, K. M., Jr. *J. Am. Chem. Soc.* **2001**, *123*, 9867−9879.
(51) Voevodin, Vl.V.; Zhumatiy, S. A.; Sobolev, S. I.; Antonov, A. S.; Bryzgalov, P. A.; Nikitenko, D. A.; Stefanov, K. S.; Voevodin, Vad. V. *Open Systems J. - Moscow* **2012**, 36−39.